JOURNAL OF PETROLEUM GEOMECHANICS
(JPG)

Original article

Permeability Prediction from Log Data using Machine Learning Methods

Mohammad Ali Davari [1], Saeedeh Senemari [1], Andisheh Alimoradi [1*], Seyed Javad Safavi [2]

1- Imam Khomeini International University, Qazvin, Iran
2- Pars Petro Zagros (PPZ) Company, Tehran, Iran

Received: 25 November 2023; Accepted: 16 December 2023

DOI: 10.22107/JPG.2024.426878.1220

Keywords

Petrophysical Interpretation, Permeability, Artificial Intelligence Network, Multi-Resolution Graph-based Clustering, Extreme Machine Learning

Abstract

In this paper, models for permeability prediction of oil reservoirs using a machine learning approach and petrophysical data are compared. Various machine learning methods, including multi-resolution graph-based clustering, conventional artificial neural networks and Extreme Learning Machines are employed to have a comprehensive comparison. RCAL data from one of Iran's oil reservoirs was used to develop and test the machine-learning approach. The results of the machine learning models employed in this paper are compared with relevant real petrophysical data and well evaluations. Seven input models of two different wells of this reservoir were considered for permeability estimation. The input logs data of models include Resistivity (RT), Effective Porosity (PHIE), Density log (RHOB), Sonic log (DT) and Compensated neutron porosity log (NPHI) logs data. The correlation coefficient and the root mean square error between the prediction data and core data in the ELM method were obtained as 0.94 and 0.06, respectively. In the MRGC method, the correlation coefficient and the root mean square error between the prediction data and core data were obtained as 0.98 and 0.09, respectively. The obtained results in this paper show that the mentioned models are well able to estimate permeability values in all parts of the studied formation and it can be concluded that the clustering method based on MRGC has more correlation with the core data, and Instead, the ELM method has the least amount of error in permeability prediction. According to the error values, ELM can be recommended as the final selected algorithm for permeability prediction in this study.

1. Introduction

The application of intelligent systems is imperative in instances where mathematical modeling is unfeasible [1]. This necessity arises from either incomplete knowledge of all parameters involved in a given process or the intricate nature of the relationships between these parameters, rendering system modeling through traditional mathematical means impractical. In such scenarios, artificial intelligence serves the purpose of observing and emulating the behaviour of the system [2,3]. Within this domain, numerous studies have been undertaken, including the utilization of neural networks for the prediction and estimation of porosity [4], the application of seismic data and artificial neural networks for porosity prediction [5], the integration of seismic data into neural networks for the determination of reservoir parameters [6]. Nooruddin has developed a model for predicting permeability based on artificial neural networks, employing laboratory measurements and capillary injection of mercury as input data [7]. Furthermore, Al-Anazi has demonstrated that support vector regression can effectively predict permeability and porosity for a sandstone reservoir with

*** Corresponding Author:** alimoradi@eng.ikiu.ac.ir

multiple data samples [8]. Additionally, Singh has employed artificial intelligence to forecast porosity using three influencing inputs (sonic, density, and resistivity) [9].

A particularly efficient generalized model, named extreme machine learning, has been introduced, boasting a swifter processing speed compared to vector networks [10]. Moreover, Safarzadeh & Shadizadeh have investigated the support vector regression method for prediction, analyzing permeability using resistivity, neutron, density, gamma rays, and acoustic profiles [11].

Olatunji et al. have also developed an extreme machine learning model and proposed a permeability estimation model utilizing an extreme machine learning approach [12]. Additionally, Xiao et al. have presented an extreme machine learning model featuring multiple hidden layers [13]. Adeniran has conducted a study on permeability determination in both homogeneous and heterogeneous reservoirs, employing data clustering techniques within the domain of oil and gas fields [14]. Zhang has employed univariate prediction model (UPP), bivariate prediction model (BPP), support vector regression (SVR), random forest (RF), and deep residual neural network (ResNet) methods to estimate permeability in sandstone [15].

The objective of this study is to develop a robust predictive model for formation permeability through the integration of petrophysical log data and core data. The aim is to design an intelligent network that demonstrates high accuracy in permeability prediction, ensuring that the methods employed yield satisfactory results with minimal error, and can be reliably applied to the entirety of the reservoir [16], [17].

2. Data and methodology

2.1. Artificial Neural Networks method (ANN)

Artificial Neural Networks (ANN) are systems that are mathematically designed to receive, process and stimulate information. This network has two main components: nodes (or neurons) and connections (which are weighted links between neurons). Each simple network includes an input layer, Hidden layer, and an output layer as showed in Fig. 1. The input layer receives signals from the external environment (or other neurons). The Hidden layer gathers and processes the input signals. These signals are transferred to the output layer and transmitted again [18,19].

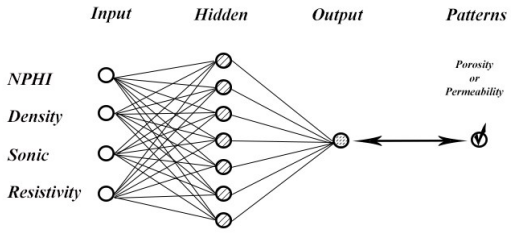

Fig. 1. The structure of the ANN

ANN method has several advantages over conventional statistical and deterministic methods. The most important of them is that it is beyond the limitations of a specific performance form. Here, methods, rules or formulas are not considered and the only question is what kind of input data the neural network can use to create a connection with the desired output. In addition, unlike linear regression models, the ANN approach does not force the predicted values to be close to the mean values and therefore preserves the true variability of the data [20].

In the ANN method, learning is a type of supervised learning that requires two groups of parameters. Independent parameters and dependent parameters. The task of the neural network is to correctly estimate the dependent parameter with the help of independent parameters.

In fact, the neural network predicts permeability with the help of independent parameters, which are the values obtained from common well logs and core (permeability) data. Due to the fact that here the type of network learning is supervised learning. Therefore, to train the network, the measured permeability data is needed. These data are used as the target parameter to adjust the network elements for the correct estimation of permeability .[9]

2.2. Multi-Resolution Graph-based Clustering method (MRGC)

The multi-resolution graph-based clustering method (MRGC) is actually a combination of artificial intelligence techniques and a hierarchical clustering method. This method has

advantages such as the ability to identify natural patterns in electrical diagrams, no need for prior knowledge about the data, automatic suggestion of the best number of clusters, the least parameters and insensitivity to their changes, and no restrictions on the type, number of data and clusters [21]. This method uses the parameters of the Kernel Representative Index (KRI) and Neighborhood Index (NI), which, in turn, differentiates it from conventional methods. The Neighborhood Index is obtained from the rank of each data relative to the desired data. The Neighborhood Index parameter replaces the distance parameter as equation 1. When the two points are close to each other, they can be easily separated from each other based on their high NI.

KRI index is a combination of NI function, distance and weighted distance M(x,y) as shown in equation 2. This index determines the degree of a neighborhood or the degree of membership in M. If this index is low, it will be affected by M. Otherwise, it has a high degree of membership and is not affected by M [21].

$$NI(X) = \sum_{N=1}^{n-1} \exp(-m) \quad (1)$$

$$KRI(x) = NI(x)M(x,y)D(x,y) \quad (2)$$

where m is the neighborhood ranking, M is the weighted distance, y is the mth neighborhood for x and D is the distance between x and y.

When the influence of the first nucleus or central point on all its neighbouring members is determined, all members are compared. Members affected by the nucleus also affect other members. Therefore, boundaries are defined where a member is influenced by its previous member, but cannot influence other members. Therefore, boundaries determine the point of division and distinguish different groups based on parameters [21].

2.3. Extreme Learning Machine method (ELM)

Extreme learning machine (ELM) is a type of single-layer feedforward neural network presented by Huang et al [10]. The ELM model includes an input layer, a hidden layer, and an output layer, which determines the input weights randomly and the output weights analytically. The ELM method includes input data, a hidden layer and output data. Theoretically, this algorithm tends to provide the best generalization performance with a very fast learning rate because it is a simple unregulated algorithm [22]. This method tends to achieve the minimum training error and also considers the weights, which is contrary to the classic gradient-based learning algorithms that only aim to achieve the minimum training error but do not consider the size of the weights. Also, unlike classical slope-based learning algorithms that only work for variable activation functions, the ELM learning algorithm can be used to train SLFNs with non-differentiable activation functions [23].

Fig. 2 contains the general network diagram of the proposed model. This model consists of input layers that receive well input values. It also has a hidden layer that includes neurons with network activation functions and ends with an output layer. The single neuron provides the final predicted permeability values.

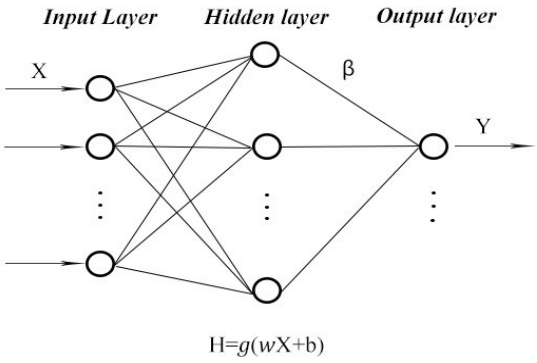

Fig. 2. The structure of the ELM

2.3.1. The learning process of the ELM method

In this methodology, the neurons of the input layer establish connections with all neurons within the hidden layer. The creation of hidden layer neurons involves the utilization of bias. The activation function for hidden neurons can be a piecewise continuous function, while for the output layer neuron, it is linear. The Extreme Learning Machine (ELM) model employs distinct algorithms to compute weights and biases, resulting in a noteworthy reduction in network

training time [24].

The behavior of neurons encompasses two essential components: the weighted sum of inputs and the activation function. Upon the application of a set of weighted input signals, activation functions are utilized to derive the response as equation 3. In this thesis, the chosen activation functions include the positive saturated linear transfer function, symmetrical saturated linear transfer function, positive linear transfer function, linear transfer function, positive hard limit transfer function, symmetric hard limit transfer function, logarithmic sigmoid transfer function, symmetric sigmoid transfer function, and Elliott symmetric sigmoid transfer function. The same activation functions are applied to neurons within the same layers, which may either be linear or non-linear. Linear functions yield a straight-line graph, while non-linear functions produce a curved line. Given that non-linear functions involve variable input and output, they commonly address classification problems. In ELM, weights and biases are randomly assigned between input and hidden layer neurons [12,25].

$$H_{jk} = g(\sum W_{ji}X_{jk}) + B_j \quad (3)$$

where j is the number of neurons in the hidden layer, i is the input neuron, k is the number of training samples, Hjk is the activation matrix of the jth hidden layer neuron for the kth training sample, g( ) is the activation function, Wji is the weight of the ith input neuron and the jth hidden layer neuron, Xjk is the input of the neuron for the kth training sample and Bj is the bias of the jth hidden layer neuron.

The matrix H is expressed as the matrix of the output hidden layer of the neural network. The weights between the neurons of the hidden layer and the output are applied using the least squares fit for the target values in the training mode against the outputs of the neurons of the hidden layer for each training example, whose mathematical equivalent can be written as equation 4 [12,25] :

$$H\beta = T \quad (4)$$

$$\beta = (\beta_1, \dots, \beta_j)_{j\times 1} \quad (5)$$

B represents the weight between the neurons of the output layer and the neurons of the hidden layer, and the vector T represents the target values for the training samples, which is expressed as equation 6:

$$T = (T_1, \dots, T_k)_{k\times 1} \quad (6)$$

Finally, the weights can be calculated from the following equation:

$$\beta = H'T \quad (7)$$

$$H(w_1, \dots, w_N, b_1, \dots, b_N, x_1, \dots, x_N) = \begin{bmatrix} g(w_1.x_1 + b_1) & \cdots & g(w_N.x_1 + b_N) \\ \vdots & \ddots & \vdots \\ g(w_1.x_N + b_1) & \cdots & g(w_N.x_N + b_N) \end{bmatrix}_{N\times N} \quad (8)$$

$$\beta = \begin{bmatrix} \beta_1^T \\ . \\ . \\ . \\ \beta_N^T \end{bmatrix}_{N\times m} \quad (9)$$

$$\mathrm{T} = \begin{bmatrix} T_1^T \\ . \\ . \\ . \\ T_N^T \end{bmatrix}_{N\times m} \quad (10)$$

where x, w, b and β are the weight vectors between the neurons of the hidden layers and the hidden layer and H' is the inverse Moore-Penrose matrix H. The T matrix is the vector between the weights of the training [12].

2.3.2. Data preprocessing in ELM

Before starting the training, in order to achieve a network with higher efficiency, pre-processing was done with the help of special functions on the inputs and outputs, after applying them, the input and output data were scaled and within a specific range. (Between 0 and 1+) were placed. One of the reasons for emphasizing the normalization of the data in this range is that the stimulus functions (such as the sigmoid function) cannot distinguish between very large values. This makes network training difficult. Obviously, after the completion of the simulation, the reverse of the above functions has been applied. Equation 11 was used to normalize the data:

$$X_n = \frac{X - X_{min}}{X_{max} - X_{min}} \quad (11)$$

In that, X_n is the normalized data, X is the initial data, X_{min} is the lowest amount of data, and $X_{max}$is the highest amount of data.

2.3.3 Data preparation

Petrophysical evaluation is the science of interpreting the information obtained from well logging, which is one of the factors in determining the characteristics of hydrocarbon reservoir rocks. The purpose of petrophysical evaluation is to calculate the petrophysical parameters of the formation such as porosity, permeability, water and oil saturated shale volume and mineral volume. Petrophysical evaluation plays an important role in evaluating the productivity of the well and ultimately the amount of hydrocarbon in situ. Petrophysical evaluation is carried out by two definite and probable methods.

Probabilistic petrophysical method or MULTIMIN is based on statistics and probability and provides statistical solutions. This method provides evaluation by using all the available logs at the same time. Therefore, its random errors are less. In this study, the multimine module of geolog software was used to evaluate the raw data obtained from well logging.

In the studied field, after collecting the required data, the information related to the logs of wells A and B were prepared and then the probability method was considered for performing the calculations. Data preparation was done in four stages: data loading, quality control and data editing, calculation of required parameters before the main calculation and environmental corrections, and then its petrophysical model was built.

Using the data related to the logs and the RCAL data available in wells A and B in the studied formation, at first to determine the permeability using ANN and MRGC models in Geolog software, and ELM model in MATLAB software. has been discussed, and then the obtained results have been compared with each other in order to achieve the best relationship and permeability diagram.

Core data statistics for each of the wells are listed in Table 1. PHIE, DT, RHOB, RT, NPHI and core permeability data of both wells A and B were used to estimate permeability. In this method, the data of both wells were used simultaneously in order to reach the most suitable model. In Table 2, all the models used in the above logs are listed in the order of use [26] , [27].

Table 1. Core data

Wells	Interval (m)	Mean permeability (mD)	Number of core data
Well A	3816-4116	0.74	98
Well B	3546-3939	1.20	301

Table 2. Input models

Model name	Independent parameters
RPDS	RT-PHIE-RHOB-DT
RPS	RT-PHIE-DT
DSP	PHIE-DT-RHOB
NDP	PHIE-RHOB-NPHI
NSP	PHIE-DT-NPHI
RDP	PHIE-RT-RHOB
PR	RT-PHIE

Seventy percent of the entire dataset was allocated for training purposes, with an additional 20% reserved for validation, leaving the remaining portion for network testing. The rationale behind assigning a substantial percentage for training lies in the network's capacity to comprehend input-output patterns and adapt to diverse conditions. The training process involves exposing the network to training data, periodically assessing its performance with validation data, and ultimately evaluating its generalization capabilities through dedicated network testing data.

3. Data processing

3.1. ANN method

The depicted flow chart of the Artificial Neural Network (ANN) method is presented in Fig. 3. Fig. 4 and Fig. 5 showcase the application of the ANN method, encompassing the training, construction, and subsequent results for each of the seven models detailed in Table 2. The models were applied to both wells, A and B. Importantly, all seven models exhibited a favorable alignment

with the permeability data obtained from the cores. Moreover, these models provided accurate estimations of permeability in instances where core data was not available.

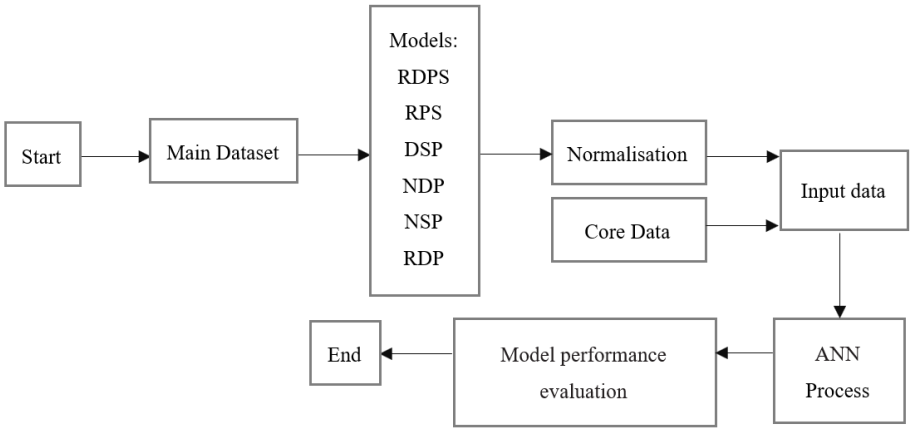

Fig. 3. Flow chart showing the steps of ANN algorithm

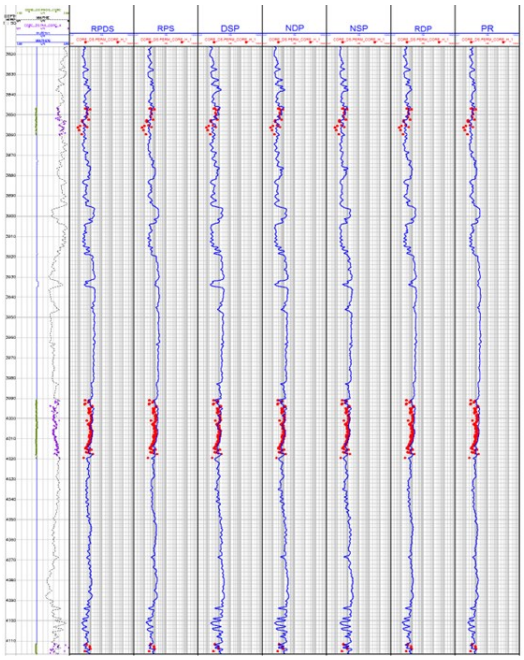

Fig. 4. predicted logs for permeability using ANN method for well A. The first column corresponds to the vertical depth relative to the surface. The second column displays the effective porosity next to the core porosity data. The third to ninth columns also show permeability estimations by ANN method using PR, RDP, NSP, NDP, DSP, RPS and RPDS models along with core permeability data.

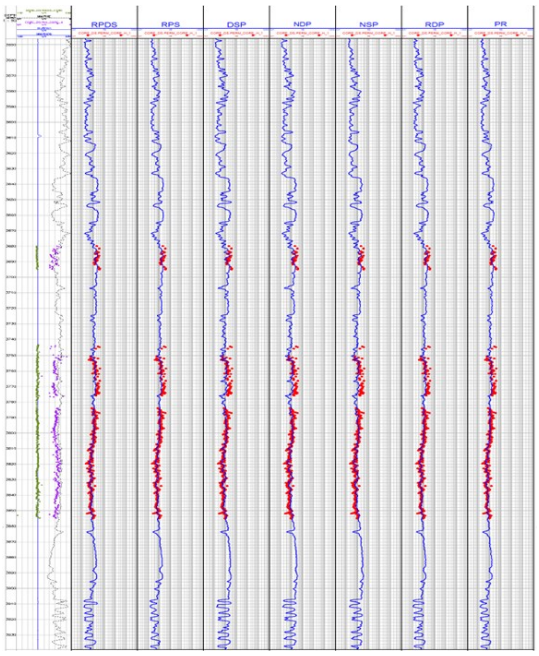

Fig. 5. predicted logs for permeability using ANN method for well B. The first column corresponds to the vertical depth relative to the surface. The second column displays the effective porosity next to the core porosity data. The third to ninth columns also show permeability estimations by ANN method using PR, RDP, NSP, NDP, DSP, RPS and RPDS models along with core permeability data.

3.1.1. ANN models results

To juxtapose the outcomes derived from the models applied in the Artificial Neural Network (ANN) methodology, cross-plots illustrating the estimated permeability of each model in comparison to core permeability were generated. Subsequently, regressions were plotted, and the correlation coefficient for each cross-plot was calculated. the cross-plots of best model for each wells can be seen in Fig. 6 to Fig. 8. The outcomes of this comparative analysis are detailed in Table 3. To assess and validate the proposed framework and facilitate effective comparative examinations with other methodologies, standard statistical metrics were employed. These metrics encompassed the correlation coefficient (R^2) and the root mean square error (RMSE).

1. The individual datasets of RT and PHIE logs within each well exhibit a commendable correlation with the permeability data obtained from the cores. Furthermore, the correlation coefficient of the PR model utilizing data from both wells also indicates a noteworthy relationship. This constitutes a noteworthy observation.
2. Although the NPHI log data in well A demonstrates a substantial correlation with the core data of that particular well, in well B, the correlation between the NPHI log data and the core data is comparatively lower. Consequently, concerning the correlation coefficients of both wells, A and B, in NDP and NSP models, we observe diminished correlation values.
3. The correlation coefficients in the RPS and RDP models suggest a robust correlation between the data derived from RHOB and DT charts with the core data.
4. Synthesizing the aforementioned observations, and evident from the correlation coefficient of RPDS, it can be inferred that there exists a significant correlation (0.78) between PHIE, RT, DT, and RHOB data. This suggests that the most appropriate model for permeability estimation is achieved through the implementation of the Artificial Neural Network (ANN) method.

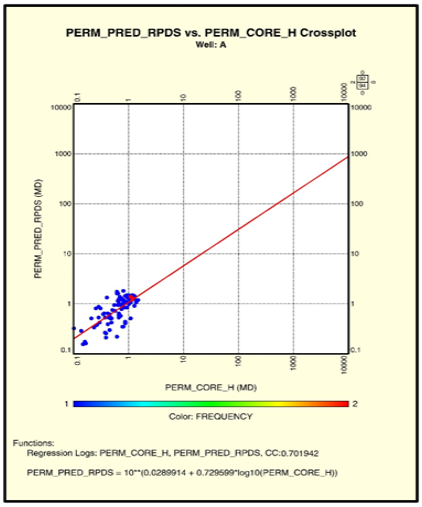

Fig. 6. Crossplot of permeability using ANN method for well A with PHIE, RT, DT and RHOB data

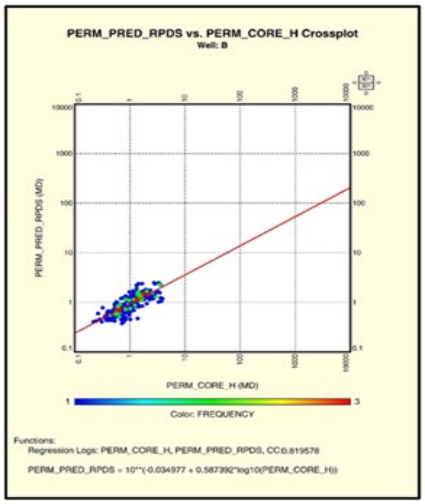

Fig. 7. Crossplot of permeability using ANN method for well B with PHIE, RT, DT and RHOB data

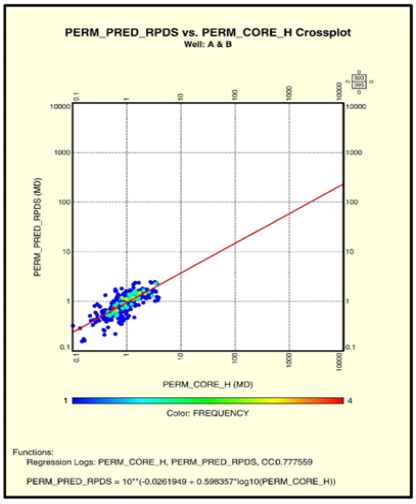

Fig. 8. Crossplot of permeability using ANN method for well A & B with PHIE, RT, DT and RHOB data

Table 3. Comparison of R2 and RMSE between the data of the models presented in the ANN method and the core data in both wells A and B

Model Name	Well A		Well B		Well A & B	
	R^2	RMSE	R^2	RMSE	R^2	RMSE
RPDS	0.71	0.36	0.82	0.55	0.78	0.51
RPS	0.72	0.54	0.34	0.58	0.72	0.57
DSP	0.72	0.34	0.61	0.67	0.65	0.61
NDP	0.76	0.33	0.58	0.68	0.66	0.61
NSP	0.77	0.41	0.56	0.69	0.63	0.63
RDP	0.74	0.46	0.81	0.57	0.75	0.55
PR	0.72	0.55	0.83	0.57	0.72	0.57

3.2. MRGC method

The flow chart of MRGC method shown in Fig. 9. The models in Table 2 are estimated by MRGC method and the obtained estimated permeability can be seen in Fig. 10 and Fig. 11.

3.2.1. MRGC models

In order to compare the results obtained from the models used in the MRGC method, the estimated cross-plots of each model with core permeability drawn. Then its regression was plotted and using the correlation coefficient of each of the cross-plots, all seven presented models were compared, the cross-plots of best model for each wells can be seen in Fig. 12 to Fig. 14, the results of which are as described in Table 4.

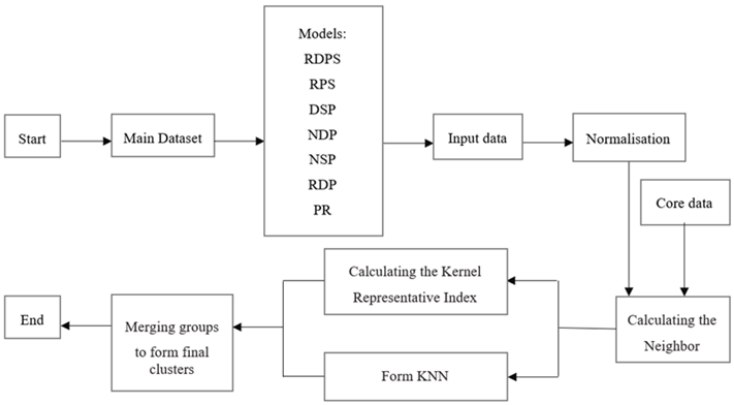

Fig. 9. Flow chart showing the steps of MRGC algorithm

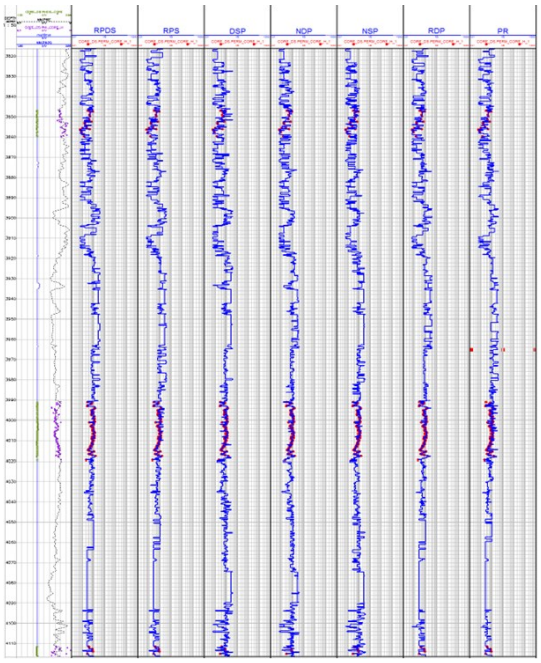

Fig. 10. predicted logs for permeability using MRGC method for well A. The first column corresponds to the vertical depth relative to the surface. The second column displays the effective porosity next to the core porosity data. The third to ninth columns also show permeability estimations by MRGC method using PR, RDP, NSP, NDP, DSP, RPS and RPDS models along with core permeability data.

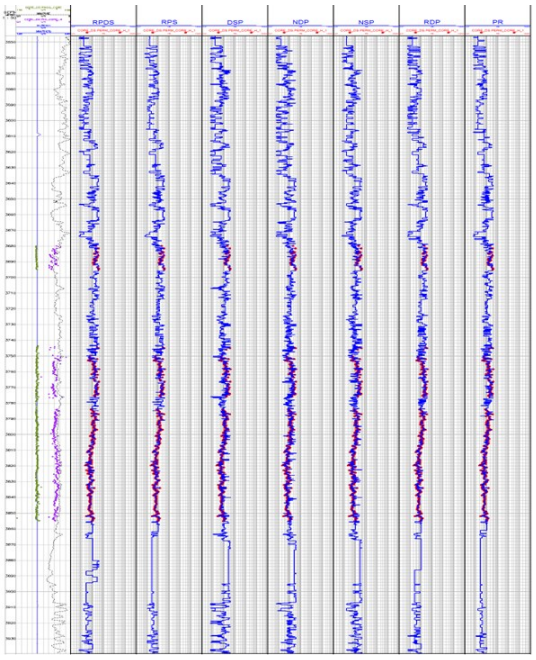

Fig. 11. predicted logs for permeability using MRGC method for well B. The first column corresponds to the vertical depth relative to the surface. The second column displays the effective porosity next to the core porosity data. The third to ninth columns also show permeability estimations by MRGC method using PR, RDP, NSP, NDP, DSP, RPS and RPDS models along with core permeability data.

3.2.2. The results obtained from the cross-plot of MRGC models with core permeability

1. Analogous to the findings of the Artificial Neural Network (ANN) method, the datasets derived from the RT and PHIE logs within each well exhibit the highest correlation with the permeability data acquired from the cores. This relationship is further affirmed by the correlation coefficient of the PR model utilizing data from both wells.

2. Despite the NPHI log data demonstrating a robust correlation with the core data of well A, the

correlation between the NPHI log data and the core data of well B is comparatively lower. Consequently, the correlation coefficients of both wells, A and B, in NDP and NSP models reflect diminished correlation values.

3. Examination of the correlation coefficients in the RPS and RDP models suggests a strong correlation between the data obtained from RHOB and DT charts and the corresponding core data.

4. A comparative analysis of the RPS and DSP methods leads to the conclusion that the influence of DT is more pronounced than that of RHOB.

5. Synthesizing the foregoing observations, and evident from the correlation coefficient of RPDS (0.987), the most substantial correlation among the graph data is observed from PHIE, RT, DT, and RHOB from right to left. This signifies that the most suitable model for permeability estimation is achieved through the Modified Robust Genetic Clustering (MRGC) method.

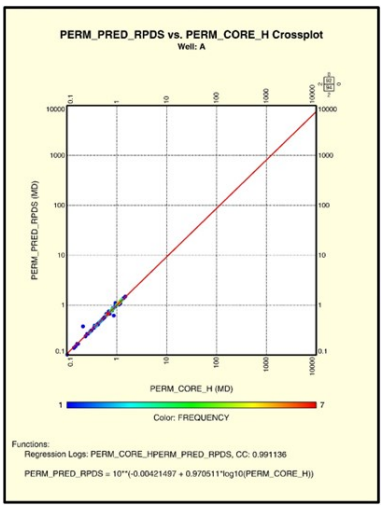

Fig. 12. Crossplot of permeability using MRGC method for well A with PHIE, RT, DT and RHOB data

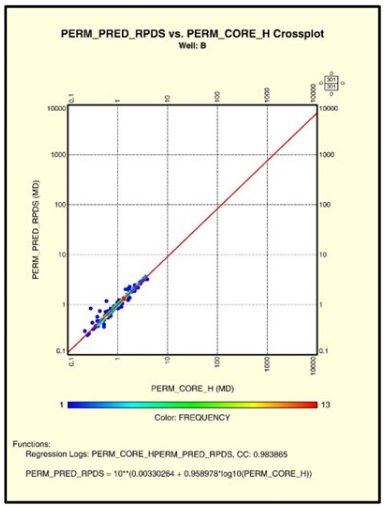

Fig. 13. Crossplot of permeability using MRGC method for well B with PHIE, RT, DT and RHOB data

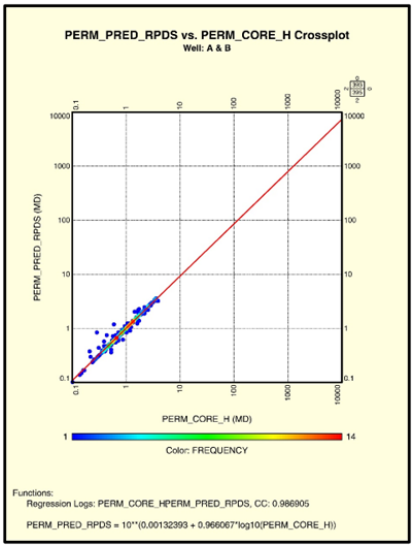

Fig. 14. Crossplot of permeability using MRGC method for well A & B with PHIE, RT, DT and RHOB data

Table 4. Comparison of R2 and RMSE between the data of the models presented in the MRGC method and the core data in both wells A and B

Model Name	Well A		Well B		Well A & B	
	R^2	RMSE	R^2	RMSE	R^2	RMSE
RPDS	0.99	0.04	0.98	0.11	0.987	0.09
RPS	0.97	0.12	0.98	0.10	0.98	0.10
DSP	0.84	0.26	0.79	0.51	0.83	0.47
NDP	0.89	0.17	0.81	0.50	0.85	0.44
NSP	0.85	0.31	0.81	0.50	0.84	0.46
RDP	0.93	0.20	0.91	0.32	0.92	0.30
PR	0.98	0.20	0.91	0.14	0.96	0.16

3.3. ELM method

The Extreme Learning Machine (ELM) network was implemented using the MATLAB program. Each of the models (PR, RDP, NSP, NDP, DSP, RPS, and RPDS) outlined in Table 2 was individually modeled for well A, well B, and the combined data from both wells. This resulted in the creation of 21 distinct models, each employing the ELM method. The network design involved a trial-and-error approach to determine the optimal number of activation functions and different neurons. The flow chart detailing this model is presented in Figure 15. The training data were input into the networks, and throughout the learning process, the learning rate of the network was regularly assessed using validation data. Validation procedures were iteratively conducted for each considered model. The resultant outcomes are summarized in Table 5. The obtained results indicate the acceptability of each of the 21 different models, thereby demonstrating the efficacy of the ELM method.

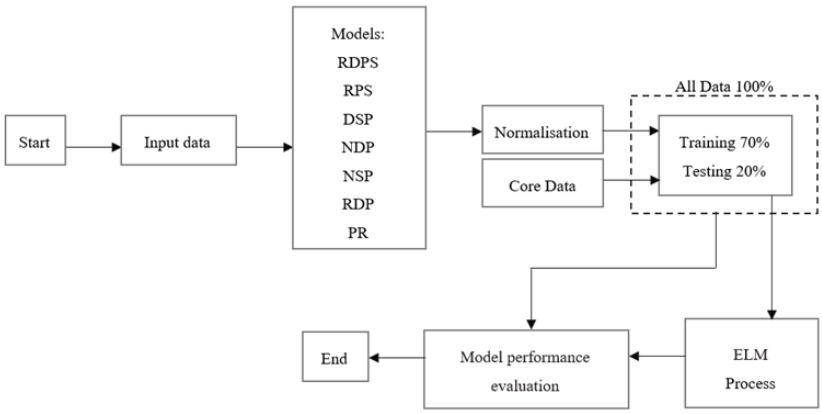

Fig. 15. Flow chart showing the steps of MRGC algorithm

Table 5. Comparison of R2 and RMSE between the data of the models presented in the ELM method and the core data in both wells A and B

Models name	Wells	Train Section		Test Section		Validation Section		Validation Data	
		R2	RMSE	R2	RMSE	R2	RMSE	R2	RMSE
RPDS	ALL	0.99	1.1264E-11	0.77	0.1100	0.76	0.1109	0.94	0.0600
	A	0.99	9.1691E-12	0.91	0.0980	0.74	0.1926	0.94	0.0762
	B	0.99	9.0029E-12	0.7	0.1200	0.55	0.1794	0.92	0.0781
RPS	ALL	0.99	1.0157E-11	0.72	0.1533	0.67	0.1473	0.89	0.0831
	A	0.99	1.1708E-11	0.74	0.2674	0.65	0.2474	0.83	0.1432
	B	0.99	1.0806E-11	0.77	0.1637	0.87	0.0995	0.92	0.0794
DSP	ALL	0.99	1.2185E-11	0.31	0.2071	0.36	0.2229	0.8	0.1162
	A	0.99	9.5897E-12	0.85	0.1166	0.75	0.1587	0.95	0.0728
	B	0.99	1.1118E-11	0.54	0.1764	0.33	0.2406	0.85	0.1095
NDP	ALL	0.99	9.1523E-12	0.38	0.2179	0.37	0.2138	0.8	0.1183
	A	0.99	6.1087E-12	0.61	0.2241	0.75	0.1786	0.87	0.1153
	B	0.99	1.2676E-11	0.53	0.2015	0.42	0.2015	0.84	0.1100
NSP	ALL	0.99	1.0217E-11	0.5	0.1712	0.57	0.1934	0.86	0.0980
	A	0.99	9.3946E-12	0.7	0.1962	0.41	0.2437	0.87	0.1175
	B	0.99	8.7451E-12	0.52	0.1838	0.47	0.2423	0.84	0.1122
RDP	ALL	0.99	0.0002762	0.64	0.1655	0.8	0.1179	0.89	0.0825
	A	0.99	9.351E-12	0.7	0.1513	0.53	0.2744	0.88	0.1114
	B	0.99	1.0711E-11	0.63	0.1664	0.6	0.2037	0.87	0.0985
PR	ALL	0.99	0.0009402	0.59	0.1780	0.64	0.1559	0.86	0.0938
	A	0.99	7.086E-12	0.14	0.2289	0.81	0.1166	0.89	0.1086
	B	0.99	0.0059912	0.61	0.1697	0.83	0.1118	0.91	0.0837

3.3.1. Results and crossplots of ELM model with core permeability

Through an exhaustive examination of results derived from diverse methods and under varying data conditions, including an analysis of the validation section in conjunction with the outcomes obtained through network implementation using well A, well B, and the combined data from both wells A and B, the RDPS method emerged as the most suitable. Specifically, when applied to the entirety of data from both wells A and B, the RDPS method demonstrated a notable correlation coefficient of 0.94 and a root mean square error of 0.0600 in the network implementation phase, contrasting with a correlation coefficient of 0.76 and a root mean square error of 0.1109 in the validation section. Given the inherent random selection of weights and biases between input and hidden layer neurons in the Extreme Learning Machine method, a meticulous evaluation of the network's efficiency and the assurance that results from the RDPS method were not merely coincidental was conducted. This involved executing the RDPS method 50 times, and the root mean square error results in the validation section are depicted in Fig. 16. This figure illustrates error values ranging from 0.06 to 0.18, substantiating the reliability of the proposed model. Based on the outcomes obtained from the training, testing, and validation processes of the RDPS model within the Extreme Learning Machine (ELM) network, and subsequent verification through 50 repetitions to ensure the reliability of the network, the

estimations of permeability were applied to both wells A and B. These results are visually presented inFig. 17 and Fig. 18.

Detailed visualizations in Fig. 19 to Fig. 24 provide diagrams and cross plots elucidating the performance of this model.

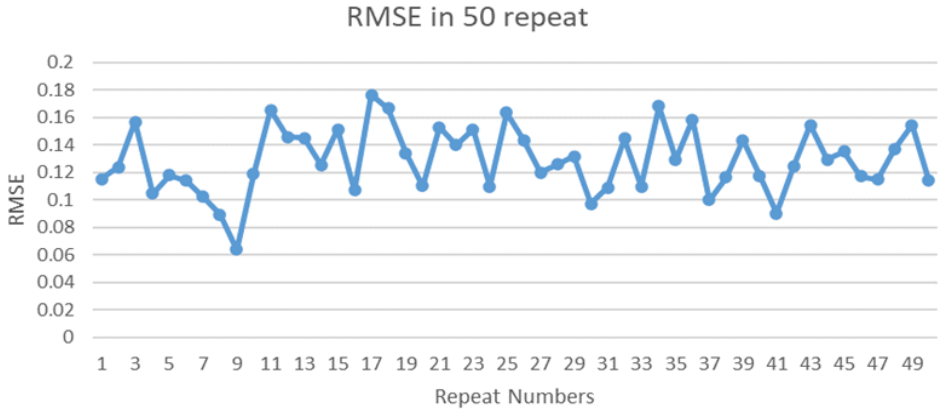

Fig. 16. Root mean square error results in the validation section in the RPDS model with 50 repetitions in the ELM network

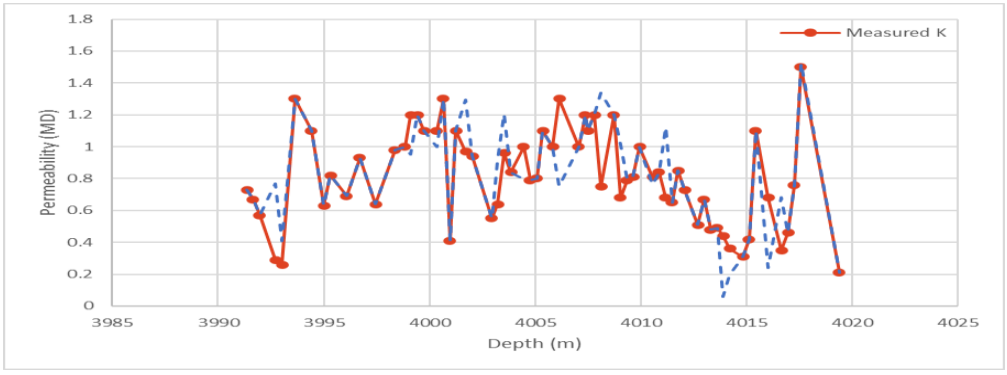

Fig. 17. Graphic matching between permeability values obtained from core and permeability estimated from RPDS model in well A with ELM method

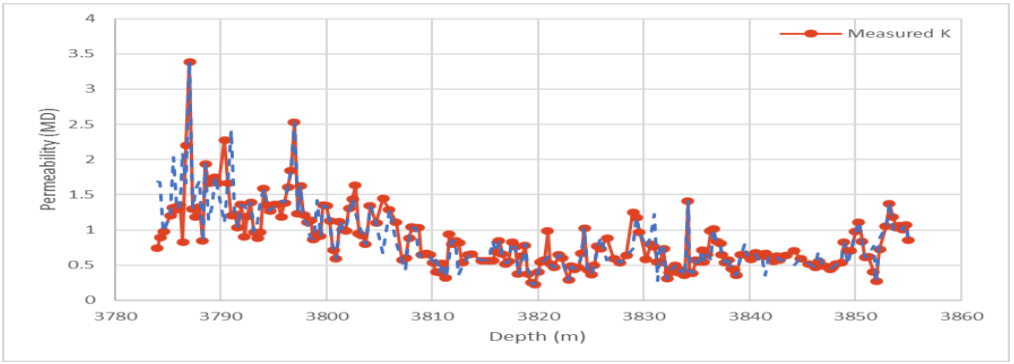

Fig. 18. Graphic matching between permeability values obtained from core and permeability estimated from RPDS model in well B with ELM method

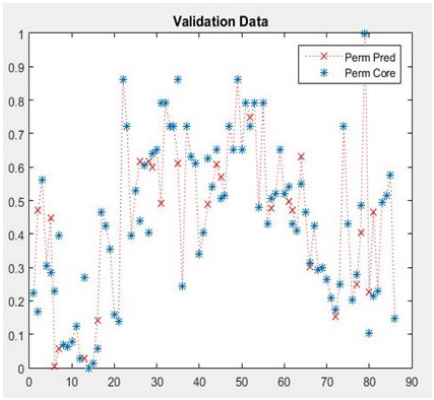

Fig. 19. Comparison between the ELM network response and the actual core permeability for Well A with PHIE, RT, DT and RHOB data

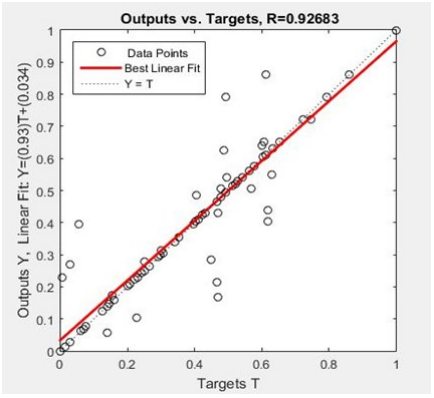

Fig. 20. Regression diagram between the ELM network response and the actual permeability of the core for Well A with PHIE, RT, DT and RHOB data

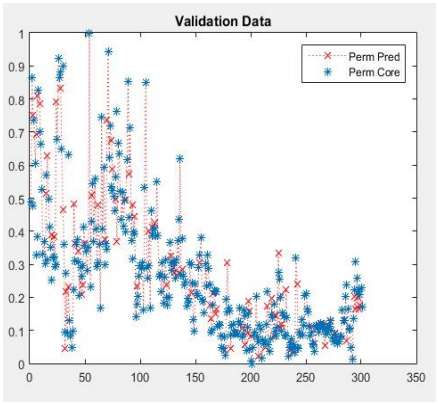

Fig. 21. Comparison between the ELM network response and the actual core permeability for Well B with PHIE, RT, DT and RHOB data

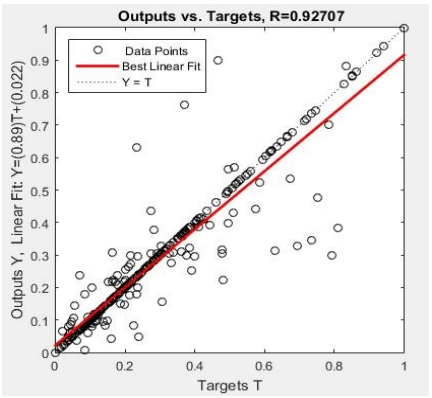

Fig. 22. Regression diagram between the ELM network response and the actual permeability of the core for Well B with PHIE, RT, DT and RHOB data

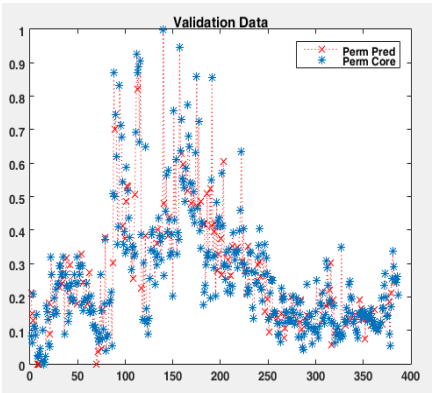

Fig. 23. Comparison between the ELM network response and the actual permeability of the core for Well A & B with PHIE, RT, DT and RHOB data

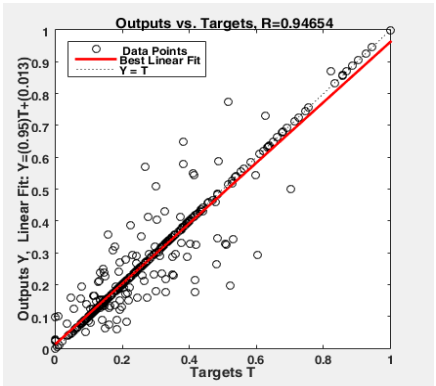

Fig. 24. Regression diagram between the ELM network response and the actual permeability of the core for Well A & B with PHIE, RT, DT and RHOB data

3.4. Discussions of Results

The intelligent systems employed in this study utilized input data comprising effective porosity, resistance, sonic, density, and neutron logs,

categorized into seven distinct models. To enhance accuracy, isomorphism was applied to permeability data, eliminating defective and damaged data.

Quantitative assessment and comparison of intelligent methods' results utilized the correlation coefficient and root mean square error. In the Artificial Neural Network (ANN) method, effective porosity and resistance exerted the greatest influence on permeability estimation, followed by density and acoustic data, with neutron data exhibiting the least impact. The RDPS model, incorporating resistivity, effective porosity, density, and acoustic parameters in the input data, yielded the most favorable estimation results. Due to the variable ranges of each of the input parameters, linear regression methods such as ANN provided weaker results than other methods.

Multi-Resolution Graph-based Clustering (MRGC) method, employing clustering to group similar permeability data, demonstrated superior results. These findings corroborated the relationships observed in the ANN method, with the RPDS model achieving the best outcome, characterized by a correlation coefficient of 0.98 and a root mean square error of 0.09. Among the permeability models created, the RPDS model, particularly in the MRGC method, emerged as the most effective.

In the Extreme Learning Machine (ELM) method, the input data underwent normalization before being implemented across seven models for well A, well B, and both wells A and B, resulting in 21 distinct states. The correlation coefficient and root mean square error for each of these states were assessed in the training, testing, and validation sections. The optimal result was associated with the RPDS model, attaining a correlation coefficient of 0.94 and a root mean square error of 0.06, utilizing input data from both wells A and B. The best results from each of the ANN, MRGC and ELM methods are given in Table 6.

In the ELM network, the weights and biases between the input and hidden layer neurons have been chosen randomly, as a result, this method, in addition to the desired result, has less error and high calculation speed. The lowest error value was related to the ELM method with the root mean square error of 0.06 and the correlation coefficient value of 0.94.

Table 6. R2 and RMSE of each method for permeability prediction

Method	R2	RMSE
ANN	0.78	0.51
MRGC	0.987	0.09
ELM	0.94	0.06

4. Conclusion

This paper proposes an integration of ANN, MRGC and ELM methods for determining core permeability from conventional well logs. By examining the results of each of the seven presented models and comparing them with each other, it was found that the input data of useful porosity and resistance had the greatest impact on permeability estimation, followed by density and acoustic data. The least impact is related to neutron data. By examining the results, the best estimation result was related to the RDPS model, which used resistance, effective porosity, density, and acoustic parameters in the input data.

• The RPDS model in all three methods, ANN, MRGC and ELM, has the most agreement and correlation with core data

• In the MRGC method, better results were obtained due to the use of clustering and dividing permeability data with values close to each other into one cluster.

• The highest value of correlation coefficient is related to MRGC method with a correlation coefficient value of 0.987 and root mean square error of 0.09.

• In the ELM network, the weights and biases between the input and hidden layer neurons have been chosen randomly, as a result, this method, in addition to the desired result, has less error and high calculation speed.

• The lowest error value was related to the ELM method with the root mean square error of 0.06 and the correlation coefficient value of 0.94.

5. References

[1] Alimoradi, A., Hajkarimian, H., Hemati Ahooi, H., and Salsabili, M., (2022), "Comparison between the Performance of Four Metaheuristic Algorithms in Training a Multilayer Perceptron Machine for Gold Grade Estimation," International Journal of Mining and Geo-Engineering, 56, 2, pp. 97–105.

[2] Mohaghegh, S., (2000), "Virtual-Intelligence Applications in Petroleum Engineering: Part 1—Artificial Neural Networks," Journal of Petroleum Technology, 52, 09, pp. 64–73.

[3] Mohaghegh, S. D., (2000), "Virtual Intelligence and Its Applications in Petroleum Engineering; Part 3. Fuzzy Logic, Distinguished Author Series," Journal of Petroleum Technology (JPT).

[4] Huang, Z., and Williamson, M. A., (1997), "Determination of Porosity and Permeability in Reservoir Intervals by Artificial Neural Network Modelling, Offshore Eastern Canada," Petroleum Geoscience, 3, 3, pp. 245–258.

[5] Hampson, D. P., Schuelke, J. S., and Quirein, J. A., (2001), "Use of Multiattribute Transforms to Predict Log Properties from Seismic Data," Geophysics, 66, 1, pp. 220–236.

[6] Russell, B. H., (2004), ″The Application of Multivariate Statistics and Neural Networks to the Prediction of Reservoir Parameters Using Seismic Attributes″, PhD Thesis, Department of Geology and Geophysics, Calgary, Alberta.

[7] Nooruddin, H. A., Anifowose, F., and Abdulraheem, A., (2013), "Applying Artificial Intelligence Techniques to Develop Permeability Predictive Models Using Mercury Injection Capillary-Pressure Data," *SPE Kingdom of Saudi Arabia Annual Technical Symposium and Exhibition*, SPE, p. SPE-168109.

[8] Al-Anazi, A. F., and Gates, I. D., (2012), "Support Vector Regression to Predict Porosity and Permeability: Effect of Sample Size," Comput Geosci, 39, pp. 64–76.

[9] Singh, S., Kanli, A. I., and Sevgen, S., (2016), "A General Approach for Porosity Estimation Using Artificial Neural Network Method: A Case Study from Kansas Gas Field," Studia Geophysica et Geodaetica, 60, pp. 130–140.

[10] Huang, G.-B., Zhu, Q.-Y., and Siew, C.-K., (2004), "Extreme Learning Machine: A New Learning Scheme of Feedforward Neural Networks," *2004 IEEE International Joint Conference on Neural Networks (IEEE Cat. No. 04CH37541)*, Ieee, pp. 985–990.

[11] Saffarzadeh, S., and Shadizadeh, S. R., (2012), "Reservoir Rock Permeability Prediction Using Support Vector Regression in an Iranian Oil Field," Journal of Geophysics and Engineering, 9, 3, pp. 336–344.

[12] Olatunji, S. O., Selamat, A., and Raheem, A. A. A., (2013), "Extreme Learning Machines Based Model for Predicting Permeability of Carbonate Reservoir," International Journal of Digital Content Technology and its Applications, 7, 1, p. 450.

[13] Xiao, D., Li, B., and Mao, Y., (2017), "A Multiple Hidden Layers Extreme Learning Machine Method and Its Application," Math Probl Eng, 2017.

[14] Adeniran, A. A., Adebayo, A. R., Salami, H. O., Yahaya, M. O., and Abdulraheem, A., (2019), "A Competitive Ensemble Model for Permeability Prediction in Heterogeneous Oil and Gas Reservoirs," Applied Computing and Geosciences, 1, p. 100004.

[15] Zhang, G., Wang, Z., Mohaghegh, S., Lin, C., Sun, Y., and Pei, S., (2021), "Pattern Visualization and Understanding of Machine Learning Models for Permeability Prediction in Tight Sandstone Reservoirs," J Pet Sci Eng, 200, p. 108142.

[16] Sarkheil, H. (2023) "Combining Voronoi Triangulation Discrete Fracture Network (DFN) Models with Fractal Dimension Analysis of Complex Sequences for Predicting Porosity and Permeability", Journal of Petroleum Geomechanics, 6 (3), pp. 74-81.

[17] Sarkheil, H., Hassani, H., & Alinia, F., (2021) "Fractured reservoir distribution characterization using folding mechanism analysis and patterns recognition in the Tabnak hydrocarbon reservoir anticline". Journal of Petroleum Exploration and Production Technology, 11, 2425–2433.

[18] Rolon, L., Mohaghegh, S. D., Ameri, S., Gaskari, R., and McDaniel, B., (2009), "Using Artificial Neural Networks to Generate Synthetic Well Logs," J Nat Gas Sci Eng, 1, 4–5, pp. 118–133.

[19] Tofighi, F., Armani, P., Chehrazi, A., and Alimoradi, A., (2021), "Comparison of the Function of Conventional Neural Networks for Estimating Porosity in One of the Southeastern Iranian Oil Fields," Journal of Petroleum Research, 31, 1400–3, pp. 90–105.

[20] Vemuri, V. R., and Rogers, R. D., (1994), "Artificial Neural Networks: Forecasting Time Series," Los Alamitos.

[21] Ye, S.-J., and Rabiller, P., (2000), "A New Tool for Electro-Facies Analysis: Multi-Resolution Graph-Based Clustering," *SPWLA Annual Logging Symposium*, SPWLA, p. SPWLA-2000.

[22] Huang, G.-B., Zhu, Q.-Y., Mao, K. Z., Siew, C.-K., Saratchandran, P., and Sundararajan, N., (2006), "Can Threshold Networks Be Trained Directly?," IEEE Transactions on Circuits and Systems II: Express Briefs, 53, 3, pp. 187–191.

[23] Huang, G.-B., Zhu, Q.-Y., and Siew, C.-K., (2006), "Extreme Learning Machine: Theory and Applications," Neurocomputing, 70, 1–3, pp. 489–501.

[24] Mantoro, T., Olowolayemo, A., and Olatunji, S. O., (2010), "Mobile User Location Determination Using Extreme Learning Machine," *Proceeding of the 3rd International Conference on Information and Communication Technology for the Moslem World (ICT4M) 2010*, IEEE, pp. D25–D30.

[25] Fathi, M., Alimoradi, A., and Hemati Ahooi, H. R., (2021), "Optimizing Extreme Learning Machine Algorithm Using Particle Swarm Optimization to Estimate Iron Ore Grade," Journal of Mining and Environment, 12, 2, pp. 397–411.

[26] Sarkheil, H., Hassani, H., & Alinia, F., (2013) "Fractures distribution modeling using fractal and multi-fractal–neural network analysis in Tabnak hydrocarbon field, Fars, Iran." Arabian Journal of Geosciences, 6, 945–956.

[27] Jahan mohammadi, H., Mosaddeg, H., Azizzadeh, M., Sarkheil, H., Mohammadnia, M., (2024), "Determination of safe mud weight window and optimal drilling path in the Gadwan formation using rock failure criteria in one of the hydrocarbon fields in southwest Iran". Journal of Petroleum Geomechanics, 6(4), 61-80.